Janus-like opposing roles of CD47 in autoimmune brain inflammation in humans and mice

May H. Han,[1] Deborah H. Lundgren,[4] Siddhartha Jaiswal,[2] Mark Chao,[2] Kareem L. Graham,[3] Christopher S. Garris,[1] Robert C. Axtell,[1] Peggy P. Ho,[1] Christopher B. Lock,[1] Joslyn I. Woodard,[1] Sara E. Brownell,[1] Maria Zoudilova,[3] Jack F.V. Hunt,[1] Sergio E. Baranzini,[5] Eugene C. Butcher,[3] Cedric S. Raine,[6] Raymond A. Sobel,[3] David K. Han,[4] Irving Weissman,[2] and Lawrence Steinman[1]

[1]Department of Neurology and Neurological Sciences, [2]Institute for Stem Cell Biology and Regenerative Medicine, and [3]Department of Pathology, Stanford University School of Medicine, Stanford, CA 94305
[4]Department of Cell Biology, Center for Vascular Biology, University of Connecticut Health Center, Farmington, CT 06030
[5]Department of Neurology, University of California, San Francisco School of Medicine, San Francisco, CA 94143
[6]Department of Pathology, Albert Einstein College of Medicine, Bronx, NY 10461

Comparison of transcriptomic and proteomic data from pathologically similar multiple sclerosis (MS) lesions reveals down-regulation of CD47 at the messenger RNA level and low abundance at the protein level. Immunohistochemical studies demonstrate that CD47 is expressed in normal myelin and in foamy macrophages and reactive astrocytes within active MS lesions. We demonstrate that CD47$^{-/-}$ mice are refractory to experimental autoimmune encephalomyelitis (EAE), primarily as the result of failure of immune cell activation after immunization with myelin antigen. In contrast, blocking with a monoclonal antibody against CD47 in mice at the peak of paralysis worsens EAE severity and enhances immune activation in the peripheral immune system. In vitro assays demonstrate that blocking CD47 also promotes phagocytosis of myelin and that this effect is dependent on signal regulatory protein α (SIRP-α). Immune regulation and phagocytosis are mechanisms for CD47 signaling in autoimmune neuroinflammation. Depending on the cell type, location, and disease stage, CD47 has Janus-like roles, with opposing effects on EAE pathogenesis.

CORRESPONDENCE
May H. Han:
mayhan@stanford.edu
OR
Lawrence Steinman:
steinman@stanford.edu

Abbreviations used: AP, acute plaque; CAP, chronic active plaque; CNS, central nervous system; CP, chronic plaque; EAE, experimental autoimmune encephalomyelitis; MOG, myelin oligodendrocyte glycoprotein; mRNA, messenger RNA; MS, multiple sclerosis.

There is prominent inflammation in myelinated regions of the central nervous system (CNS) during the acute stage of multiple sclerosis (MS; Steinman, 2004). MS is a complex disease with a heterogeneous pathology where damage and repair often occur simultaneously in the CNS tissue (Lassmann et al., 2001; Frohman et al., 2006). High-throughput analyses of genes, proteins, lipids, and antibodies had previously been undertaken to elucidate the molecular signature of MS (Lock et al., 2002; Robinson et al., 2002; Kanter et al., 2006; Han et al., 2008).

Microarray and proteomic analyses of brain lesions, cerebrospinal fluid, and immune cells of MS patients had revealed unexpected molecules and pathways involved in the disease pathogenesis (Dutta et al., 2006; Ousman et al., 2007; Han et al., 2008). However, each technique has its limitations because of the half life of the target molecules, their compartmentalization within the cell, and limitations of the platforms themselves. Moreover, direct comparison of transcriptomic and proteomic databases from different groups is complicated because of lack of standardization of techniques and the heterogeneity of tissue analyzed. We thus proposed a comparative systems biology approach to study the very same tissues from MS brain lesions using gene microarrays and mass spectrometry. This combined approach was undertaken with the hope to illuminate dynamic events that occur during disease pathogenesis.

In this study, we combined information obtained from transcriptomic and proteomic experiments of the same MS brain tissue. We compared the detection and coverage of targets from each platform and then studied the concordance of RNA and protein expression levels. One of the molecules we identified from this strategy is CD47, a target involved in important immune functions. We studied the role of CD47 in the CNS and peripheral immune system using the experimental autoimmune encephalomyelitis (EAE) model, human MS brain tissue, and in vitro assays. We demonstrated that modulating CD47 function during initiation and progression has opposing effects in the peripheral immune system and the CNS during autoimmune neuroinflammation.

RESULTS

Comparison of RNA and protein expression profiles from MS brain lesions

We compared transcriptomic and proteomic profiles from the same MS brain tissue to study differential expression of RNA transcripts and proteins during disease progression. Microarray analysis was newly performed for this study. Proteomic experiments were based on the MS brain lesion proteome dataset from our previously published work (Han et al., 2008). Tissue containing acute plaque (AP), chronic active plaque (CAP), and chronic plaque (CP) were analyzed by microarray analysis and by mass spectrometry (Fig. S1). Microarray analysis identified 6,601 RNA targets (Table S1), whereas the corresponding proteomic study identified 2,404 protein targets (Table S2). Only 1,229 RNA targets (of the 6,601 total, ∼20% of identified) mapped to 834 proteins identified in the proteomic study (∼30% of all proteins identified). The majority of the targets (5,372 RNA targets and 1,570 proteins) had no overlap between the two platforms (Fig. S2 and Table S3). We then grouped 834 common targets (identified in both microarray and proteomic platforms) into inliers

(RNA expression levels correlate with protein expression levels; relative abundance difference between RNA probe intensities and protein spectral counts were less than one order of magnitude), midliers (RNA expression levels correlate with protein expression levels; relative abundance less than two orders of magnitude), and outliers (RNA expression levels do not correlate with protein expression levels; relative abundance greater than two orders of magnitude) to study concordance between messenger RNA (mRNA) and protein expression (Lu et al., 2007). We identified 374 inliers (45%), 407 midliers (49%), and 53 outliers (6%) using this criteria (Fig. 1 and Table S3). This data for the first time suggested that only a fraction (30% of proteins and 20% of RNA) of the targets were present as both RNA and protein forms in a given tissue. However, RNA and protein expression levels correlated reasonably well when the same target was identified in both types of analyses (Gygi et al., 2000).

CD47 expression is down–regulated in active MS lesions

We identified CD47 among the targets that were down-regulated at the mRNA level and expressed at low abundance at protein levels within active MS lesions (Fig.1 [within inliers group] and Table S3 [MicroMS overlap 834, row 209, CD47 high–lighted in yellow]). CD47, a membrane protein which is expressed in immune cells and cells of the CNS, participates in diverse cellular functions by signaling via its receptors signal regulatory protein α (SIRP-α) or thrombospondin (Griffiths et al., 2009). The importance of CD47 had previously been implicated in MS, but its cellular and molecular mechanism during MS pathogenesis has yet to be elucidated (Koning et al., 2007; Junker et al., 2009).

CD47$^{-/-}$ mice are resistant to EAE

To understand the role of CD47 in autoimmune neuroinflammation, we induced EAE in CD47$^{-/-}$ mice and compared its clinical course with that of its WT counterparts. CD47$^{-/-}$ mice were refractory to EAE (Fig. 2 A), and their splenocytes
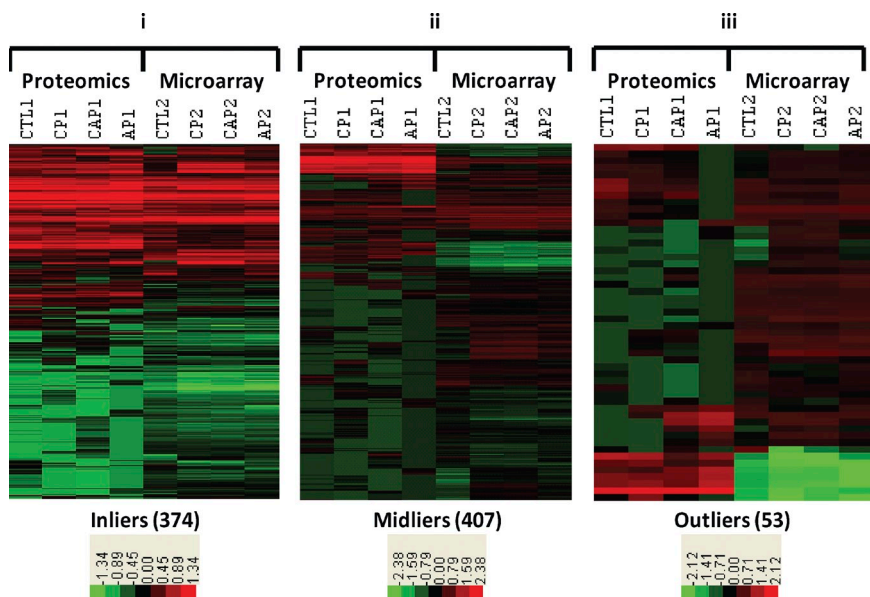

Figure 1. Identification and comparison of transcriptomic and proteomic landscapes. Comparative expression levels from the overlap of microarray and proteomic analysis of MS lesions. 834 MS UniProt IDs were jointly detected in both microarray and mass spectrometry analysis. RNA and protein expression levels of targets were measured by fluorescent intensity and spectral counts, respectively. Global transcriptomic and proteomic landscapes were compared for the 834 overlapping targets using logs (base 10) of mean relative abundance normalized to a mean of zero. Those proteins with absolute log difference <1 for each of the four lesion types (control [CTL], AP, CAP, and CP) were called inliers (i), <2 midliers (ii), and >2 outliers (iii). Note that an absolute log difference of 1 denotes a one order of magnitude difference in relative abundance.

failed to exhibit an inflammatory phenotype upon activation with myelin oligodendrocyte glycoprotein (MOG) antigen in vitro (Fig. 2 B). We adoptively transferred immune cells from immunized preclinical WT or CD47$^{-/-}$ EAE mice into naive WT or CD47-deficient mice. CD47$^{-/-}$ recipients of WT donor cells developed EAE; however, the disease was
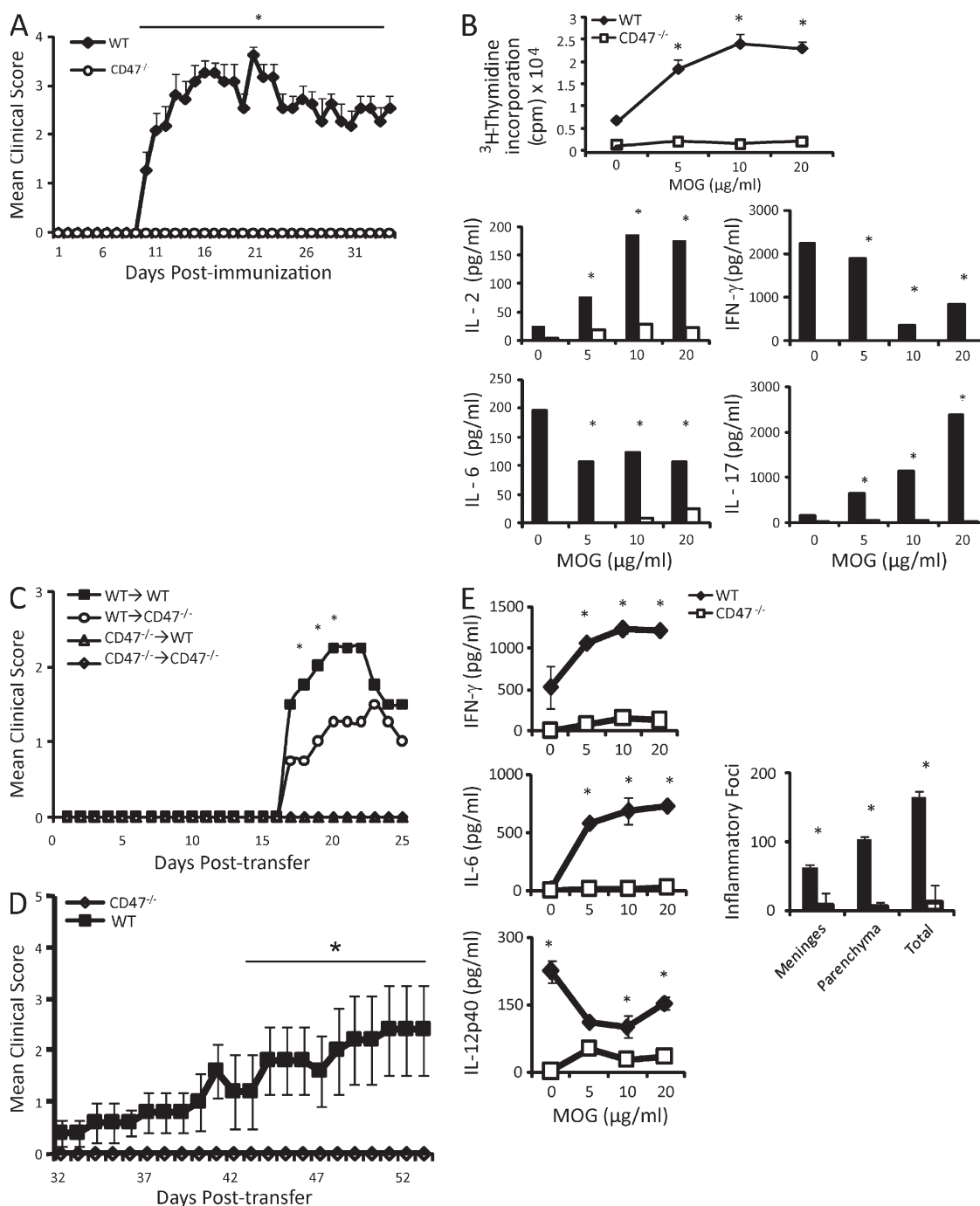
Figure 2.   CD47$^{-/-}$ mice are resistant to autoimmune neuroinflammation. (A) Mean clinical scores ± SEM of C57BL/6 WT mice or CD47$^{-/-}$ mice immunized with CFA and myelin peptide. *, P < 0.05 by Mann-Whitney analysis. (B) In vitro proliferation assay and cytokine measurement of splenocytes activated in culture with 0–20 µg/ml MOG$_{35-55}$ from WT and CD47$^{-/-}$ EAE mice. This experiment was performed three times with n = 10 mice per arm. (C and D) WT or CD47$^{-/-}$ mice were immunized with adjuvant and myelin peptide. Immune cells were harvested on day 9 and cultured in vitro with IL-12 for 5 d. Expanded T cell clones from either WT or CD47$^{-/-}$ mice were adoptively transferred into naive WT or CD47$^{-/-}$ mice (C) or naive RAG$^{-/-}$ mice (D) and followed daily for signs of EAE. This experiment was performed once with n = 5 mice per arm. *, P < 0.05 by Student's t test (in C, WT→WT vs. WT→CD47$^{-/-}$). (E) Ex vivo recall cytokine production in splenocyte cultures and degree of CNS inflammation of mice from D. Error bars were calculated from standard error of triplicate samples. *, P < 0.05.

less severe compared with WT recipients of WT donor cells (Fig. 2 C). WT recipients of CD47$^{-/-}$ donor cells did not develop EAE and remained healthy throughout the experiment. This was confirmed when we then adoptively transferred MOG-activated immune cells from either WT or CD47$^{-/-}$ into RAG$^{-/-}$ mice lacking in both T and B cells. Recipient RAG$^{-/-}$ mice transferred with CD47$^{-/-}$ donor cells were again refractory to EAE (Fig. 2, D and E).
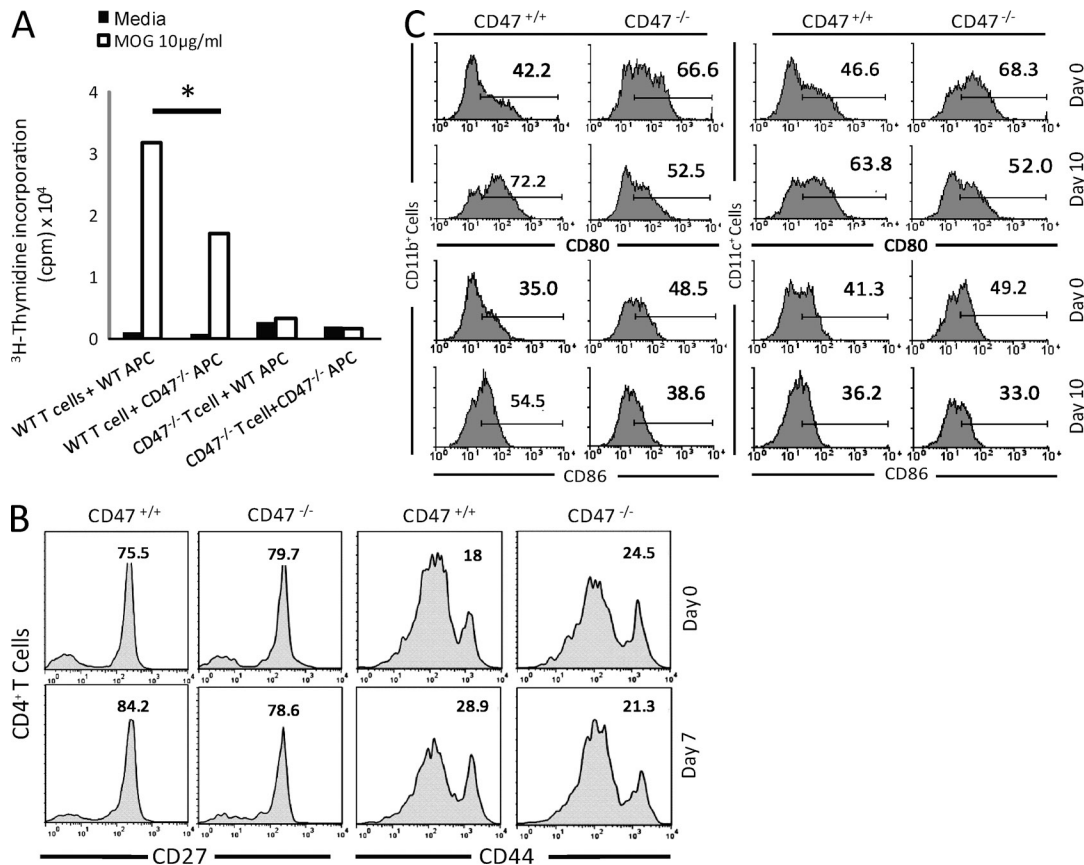
T cells and APCs are defective in CD47$^{-/-}$ mice

We performed assays to determine whether T cells or APCs from CD47$^{-/-}$ mice were defective. We co-cultured irradiated naive splenocytes from WT or CD47$^{-/-}$ mice in vitro with CD3$^+$ T cells from WT or CD47$^{-/-}$ immunized mice, reactivated with MOG peptide, and measured T cell proliferation. There was impaired proliferation with WT T cells when co-cultured with irradiated CD47$^{-/-}$ splenocytes, suggesting that both T cells and APCs lacking in CD47 were defective in generating encephalitogenic T cells (Fig. 3 A). This was confirmed by flow cytometry that T cells and APCs from CD47$^{-/-}$

mice failed to express markers of activations (CD27 and CD44 on T cells, and CD80 and CD86 on APCs) in response to active immunization with MOG$_{35-55}$ peptide in Freund's adjuvant (Fig. 3, B and C). Control experiments demonstrated that T cells and APCs from CD47$^{-/-}$ mice were capable of activation by anti-CD3/anti-CD28 or LPS and CpG (Figs. S3 and S4).

Blocking CD47 at the peak of disease worsened EAE

Based on the finding that CD47$^{-/-}$ mice were resistant to EAE, we hypothesized that blocking CD47 with mAb (mAb CD47) would ameliorate neuroinflammation. However, we observed that WT EAE mice treated with mAb CD47 by daily i.p. injections at the point of maximal paralysis worsened EAE severity compared with IgG-treated control mice (Fig. 4 A). This was accompanied by enhanced immune cell proliferation and inflammatory cytokine production in the spleens and lymph nodes (Fig. 4, B–F). In support of this finding, we observed that EAE mice treated with mAb against CD47 at the time of immunization developed less severe EAE (Fig. S5). In the bone marrow chimera experiment, CD47$^{-/-}$

Figure 3. CD47$^{-/-}$ T cells and APCs are defective in EAE induction. (A) CD3$^+$ T cells from WT or CD47$^{-/-}$ mice isolated by negative selection were cultured in vitro with irradiated splenocytes from WT or CD47$^{-/-}$ mice, pulsed with [^{3}H]thymidine for 48 or 72 h, cells were harvested, and radioactive thymidine incorporation was measured. *, P < 0.05 by Student's t test. (B and C) Effects of CD47 on the frequency of activated leukocytes during EAE. T cells (B) or APCs (C) from CD47$^{+/+}$ and CD47$^{-/-}$ mice analyzed on days 0 and 7 or 10 d after induction of EAE for CD27 and CD44 expression levels on T cells (B) and CD80 and CD86 expression levels on APCs (CD11b$^+$ and CD11c$^+$; C). (Day 0 vs. day 7 or day 10 after immunization, P < 0.05 by Student's t test). This experiment was performed twice with n = 3–5 mice per arm.
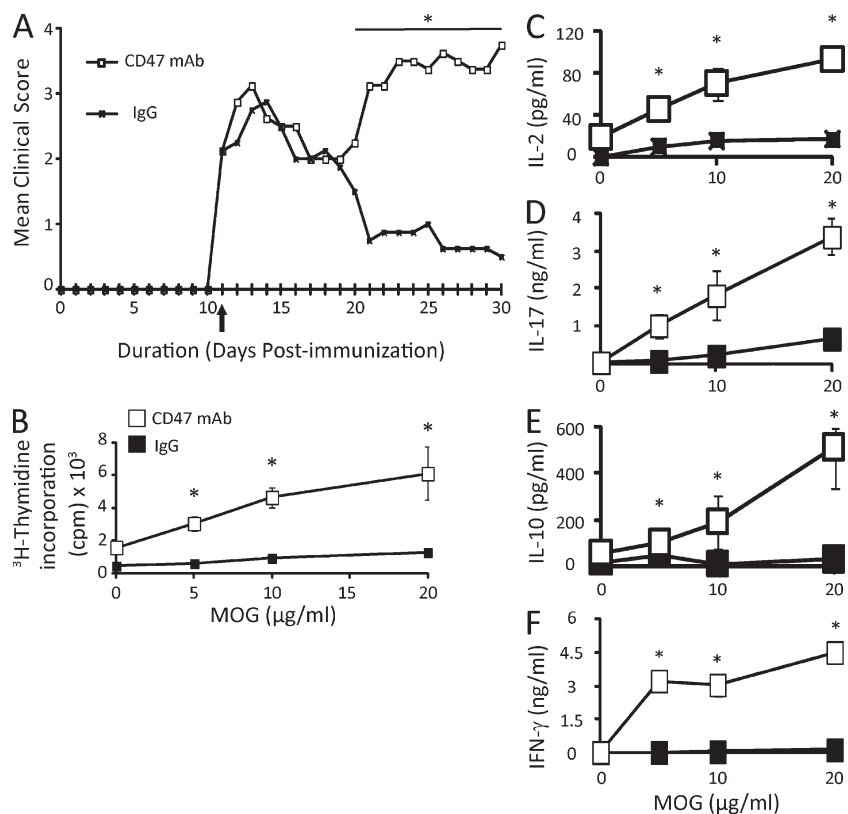
Figure 4. CD47 blockade at the peak of disease worsens EAE. (A) WT C57BL/6 mice were immunized with CFA and MOG_{35-35}. Mice were treated with daily 100-µg i.p. injections of either mAb against CD47 (mAb CD47) or control IgG. *, P < 0.05 by Mann-Whitney analysis. (B–F) Immune cells isolated from lymph nodes of either mAb CD47– or control IgG–treated mice cultured in vitro were analyzed for immune cell proliferation by means of [3H]thymidine incorporation (B) or cytokine production (C–F). This experiment was performed twice with $n = 10$ mice per arm. Error bars were calculated from standard error of triplicate samples. *, P < 0.05.

recipient mice also developed worse EAE (Fig. S6). The finding that CD47 blockade at peak worsened paralysis disease suggested that CD47 may have different functions during disease initiation and during progression of EAE.

CD47 is expressed in myelin and foamy macrophages within active MS lesions

We performed immunohistochemistry of MS brain lesions to study CD47 expression and cellular localization. CD47 was expressed mainly on the myelin of normal control brains (not depicted) and in unaffected areas within MS brains (Fig. 5 A). Within MS tissue, CD47 expression was decreased in demyelinated areas within active MS lesions (Fig. 5, B and C). CD47 immunoreactivity was observed in reactive astrocytes (Fig. 5, D and E) and in foamy macrophages (Fig. 5 F). Infiltrating immune cells, mostly CD3^{+} cells, did not express CD47 (Fig. 5, G and H).

Down–regulation of CD47 promotes phagocytosis of compact myelin and splenocytes

Engagement of CD47 to its receptor SIRP-α relays the "don't eat me" signal and prevents cells from being phagocytosed by macrophages (Jaiswal et al., 2009). Immune regulation is one of the major mechanisms by which CD47 participates in the pathogenesis of EAE. However, other potential mechanisms such as phagocytosis may also play an important role in neuro-inflammation. To test this hypothesis, we identified CD47 protein in the human brain myelin fractions by mass spectrometry.

Human brain myelin was fractionated by gradient centrifugation (Menon et al., 2003). CD47 protein was colocalized in several fractions containing myelin (main band, dispersion, and pellet fractions; Fig. 6, A–C). We then tested the effects of down-regulation of CD47 on myelin phagocytosis in an in vitro assay. Purified human myelin fraction was incubated with activated mouse macrophages, in the presence of either media alone or with blocking antibodies against CD47, SIRP-α, or isotype control IgG. There was increased phagocytosis of the myelin fraction when blocked with mAb CD47 compared with media or isotype control (Fig. 6 D). Similarly, myelin phagocytosis was also increased when blocked with anti–SIRP-α. This suggested that down-regulation of CD47 promotes demyelination in a SIRP-α–dependent mechanism in the CNS, explaining a potential mechanism (among many) for worsening EAE with down-regulation of CD47.

We observed a similar effect of CD47–SIRP-α signaling in the peripheral immune cells of EAE mice. We coated splenocytes from EAE mice with either mAb CD47 or control IgG and measured the phagocytosis index when incubated with mature mouse macrophages. We found that blockage of CD47 led to a higher phagocytosis index compared with media or with the isotype control (Fig. 6, E and F). Concurrently, a similar effect was observed when EAE splenocytes were blocked with an antibody against SIRP-α. This observation supports that CD47–SIRP-α signaling played an important role in autoimmune neuroinflammation.

DISCUSSION

Global large-scale comparisons of protein and RNA profile had previously been investigated in experimental systems (Kislinger et al., 2006; Wu et al., 2007). To our knowledge, systematic integration of multiple platforms has never been reported in a study of MS. This study used two different platforms for "-omic" analysis and provided quantitative expression patterns of genes and proteins from the same MS brain lesions. This exercise illustrated dynamic changes in mRNA and protein expression profiles. It revealed differences in outcomes for transcriptomic and proteomic platforms. It also

selected targets that were confluent with both platforms and instigated interest to perform in depth studies of molecules such as CD47. Although there were many other targets that showed concordant changes on transcriptional and proteomic platforms, we selected CD47, one of the intriguing molecules in the set, to exemplify how such large-scale profiles could shed mechanistic insights into pathophysiology. The identification of key molecules with these large-scale technological platforms covering proteins and gene transcripts was merely the first major step in understanding function.

The discordant and opposing effects of CD47 on peripheral immune cells and the CNS raised several intriguing points on the biology of CD47. Here we showed there was increased phagocytosis of myelin in the CNS when CD47 was down-regulated. However, this finding does not explain why there is peripheral immune activation in the anti-CD47–treated EAE mice (Fig. 4, B and C). One other explanation, not necessarily mutually exclusive, is that continued presentation of antigen (myelin peptide MOG) by APCs might worsen disease severity.

CD47 is ubiquitously expressed in all resident cells of the CNS, but its exact function in neurons, astrocytes, and myelin has not been examined (Cahoy et al., 2008). The novel finding of CD47 in association with compact myelin also raised several possibilities on how it might play a role in demyelinating disease. CD47, also known as integrin-associated protein might well be involved in packing the myelin sheath around axons. Whether lack of CD47 promotes demyelination in vivo by SIRP-α–dependent phagocytosis has not been investigated. Furthermore, whether removal of myelin debris is detrimental or promotes new myelin formation also remains to be answered. These important questions are currently being addressed in our laboratory by using tools such as CD47$^{-/-}$ mice in lysolecithin–induced demyelination.

Astrocytes play a crucial role in MS pathogenesis by modulating inflammation and maintaining the integrity of the blood–brain barrier and repair of demyelinating lesions (Barres, 2008). Junker et al. (2009), as well as our own experiments, suggested that reactive astrocytes in active MS lesions (and not on astrocytes in chronic MS lesions) express high levels of CD47.
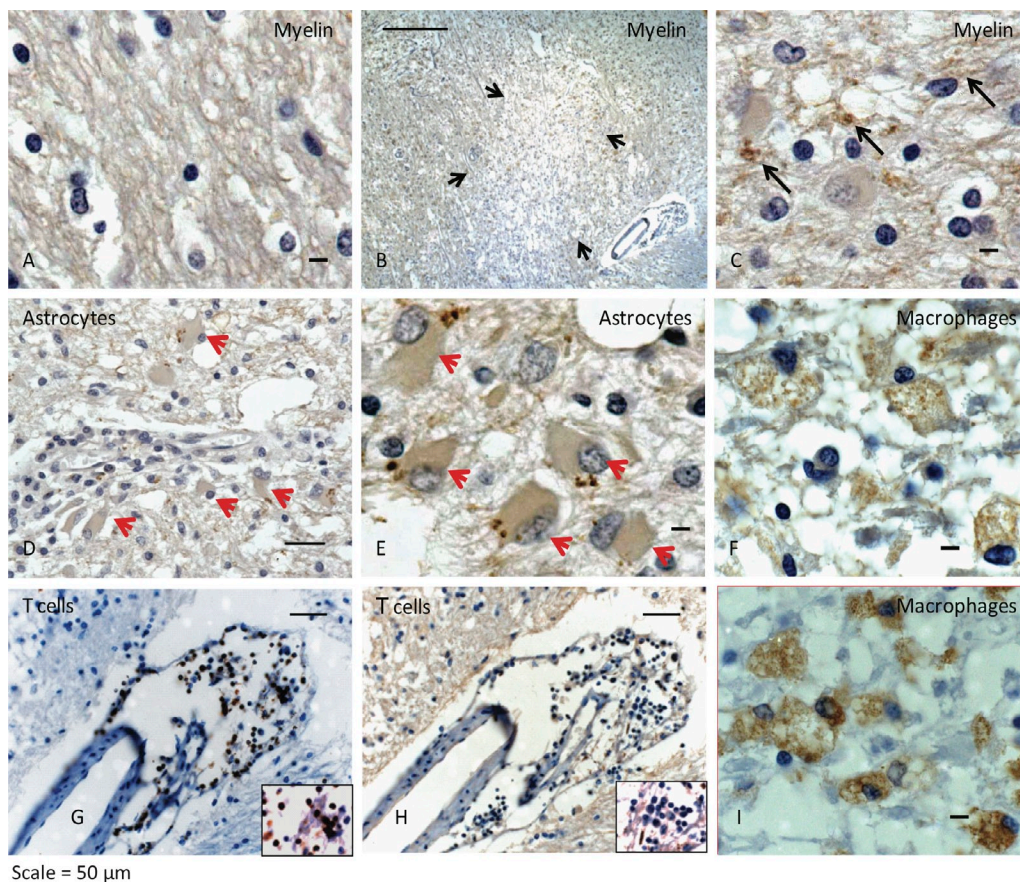

Figure 5.   CD47 is expressed in myelin, astrocytes, and foamy macrophages in active MS lesions. (A) Expression levels of CD47 in normal myelin. (B) Loss of CD47 staining in demyelinated areas. Arrows denote area of demyelination. (C) Residual myelin within the MS lesions (arrows). (D and E) CD47 staining on astrocytes (red arrows). (F) CD47 expression in macrophages. (G) Inflammatory cells within perivascular cuff staining with anti-CD3. (H) CD3+ cells showing negative staining for CD47 expression. Insets in G and H show higher magnification of CD3+ cells. (I) MS lesion stained with anti-CD68 as control for macrophages.

Findings from our immunohistochemical experiments of MS lesions are also in agreement with their findings, suggesting that CD47 in astrocytes participates in pathogenesis of auto-immune neuroinflammation.

These experiments exemplify the dual and contradictory effects of CD47 during initiation and progression of auto-immune neuroinflammation. These Janus-like opposite findings are likely caused by expression of CD47 in different cell types. Combined with the multiple signaling pathways in which CD47 is involved, we have exposed very different roles for this molecule in different contexts. We are learning this lesson repeatedly when comparing the roles of molecules like the major histocompatibility complex and complement pathway in the immune system versus the nervous system (Stevens et al., 2007; Shatz, 2009). Furthermore, we are now learning that molecules well known to the nervous system like the synaptic transmitter gamma amino butyric acid play different roles in the immune system (Bhat et al., 2010). We focused our study here on CD47–SIRP-α interactions, but other effects on inflammation may be related to CD47-Thrombospondin signaling (Lamy et al., 2007). Future studies will focus on dissecting the interplay of these pathways to study inflammatory demyelinating diseases.

This raises an important question on whether modulating CD47 has a potential role for therapy in MS. Using blocking antibody against CD47 has been shown to be beneficial in a subset of acute myeloid leukemias (Majeti et al., 2009). However, in a setting like autoimmune neuroinflammation where CD47 has opposing effects during early and late stages of disease, it would be important to decide whether blocking or replenishing CD47 may have different effects depending on disease stage. As a precedent, we should remember that immune therapies such as TNF blockade are beneficial in rheumatoid arthritis, whereas they worsen MS. Like many key players that maintain health and disease, modulating CD47 could at once be harmful and beneficial, depending on the context.
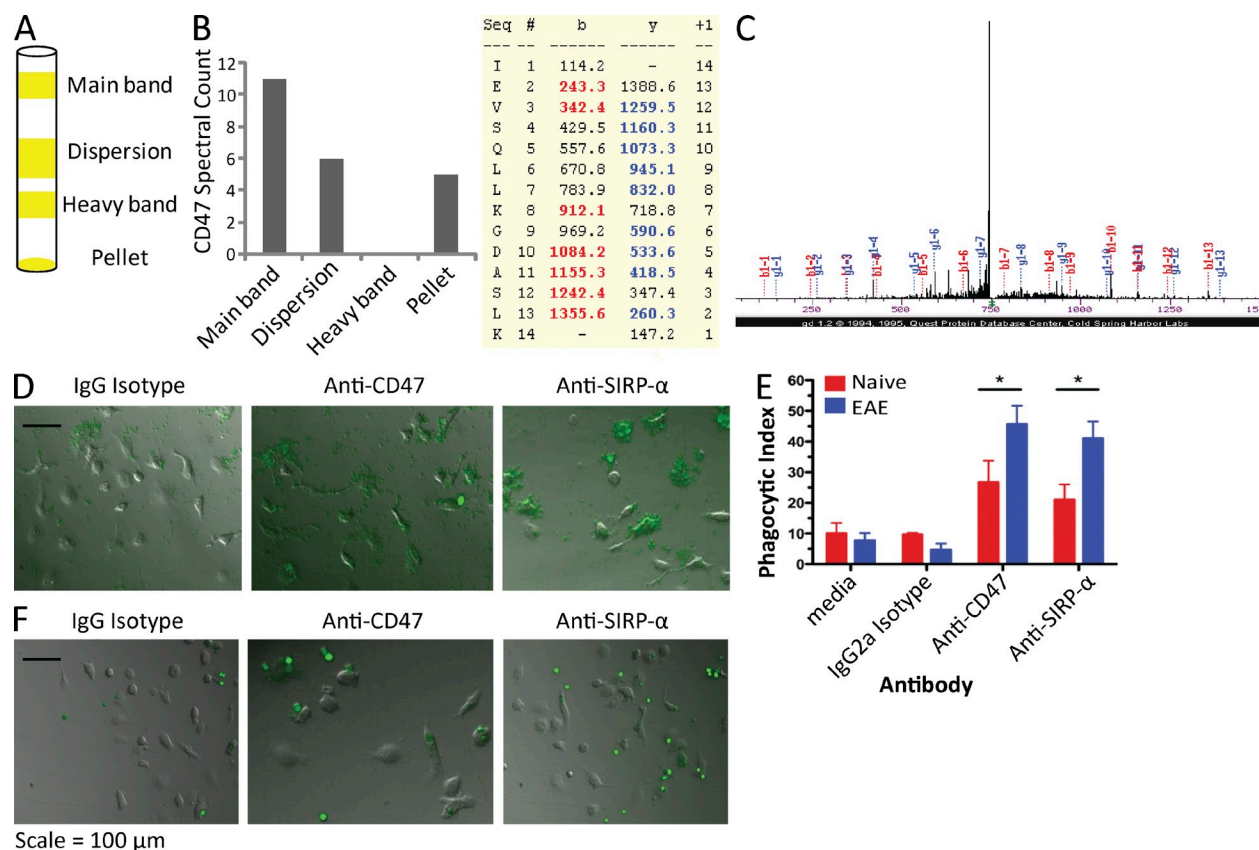
Figure 6. **Down-regulation of CD47 enhances myelin and EAE immune cell phagocytosis by a SIRP-α–dependent mechanism.** (A and B) Graph depicting CD47 expression in different myelin fractions measured by spectral count. (C) A representative spectra of CD47 peptide ions identified by mass spectrometry. (D) Purified human myelin fraction was stained with CSFE and incubated with mature mouse macrophages in the presence of control IgG, anti-CD47 blocking mAb, or anti–SIRP-α, and then phagocytosis of myelin was visualized by fluorescent microscopy. (E and F) CD47 blockade analysis of EAE immune cell phagocytosis. (E) Graph depicts EAE splenocytes phagocytosis in the presence of the indicated antibodies. Error bars were calculated from standard error of triplicate samples. *, $P < 0.05$. (F) Splenocytes from either naive or WT C57BL/6 mice immunized with myelin peptide were stained with CSFE and then pretreated with either isotype control IgG or blocking antibodies against either CD47 or SIRP-α before incubation with mature differentiated mouse macrophages. The phagocytosis index was measured by a fluorescent microscope.

MATERIALS AND METHODS

Materials. All solvents and reagents were mass spectrometry or American Chemical Society grade from Thermo Fisher Scientific. Anti-CD3 and anti-CD28 were obtained from BD. The RNeasy RNA isolation kit was purchased from QIAGEN. Human gene expression HG-U133 Plus 2.0 arrays were purchased from Affymetrix. Blocking human mAb against CD47 and mIAP301 monoclonal rat anti–mouse were provided by I. Weissman. ABC kit, secondary antibodies (biotinylated horseradish peroxidase conjugates), and diaminobenzidine (DAB) were obtained from Vector Laboratories. Monoclonal anti-GFAP (glial fibrillary acidic protein), anti-CD3, anti-CD45, and anti-CD68 were obtained from Dako. Monoclonal anti-PLP (proteolipid protein) was a gift from R.A. Sobel.

Human brain samples. Fresh-frozen archived autopsy brain samples were studied by microarray and proteomic analysis. A total of six MS and two control brain samples were included. Samples were obtained from both sexes, age range 23–54 yr, and autopsy interval varied from 4 to 24 h. Human MS brain tissue research was performed according to Institutional Review Board guidelines approved by Stanford Human Subjects Research.

Histological characterization and immunohistochemistry. Cryosections from MS and control samples were characterized into three distinct entities, AP, CAP, and CP, and stained with hematoxylin and eosin and Luxol fast blue. Immunohistochemistry was also performed on the same sections using antibodies against CD3, CD45, CD68, GFAP, and PLP as described in Han et al. (2008). Control brain samples were also analyzed in a similar fashion to rule out CNS pathology. Mouse anti–rat CD47 antibody (1:100 dilution) was used to perform immunohistochemistry of MS lesions.

Microarray experiments. Visible MS lesions from brain tissue samples were isolated, and total RNA was extracted using the RNeasy RNA isolation kit. 3–5 μg of total RNA was analyzed using Human Genome U133 Plus 2.0 arrays (Affymetrix) with duplicate arrays for each sample. Gene expression output was analyzed using the Affymetrix Expression Console, SAM (significance analysis of microarrays), Cluster, and TreeView programs (Eisen et al., 1998; Tusher et al., 2001). A total of 54,675 probe sets are represented on the arrays. Probe-level analysis was performed using the MAS5 algorithm. We then selected targets that (a) were called "present" in at least one of the seven arrays analyzed, (b) had a probe intensity of ≥100, (c) had a probe level analysis p-value <0.05, and (d) used ≥10 out of the 20 available probe pairs. Housekeeping and control genes were removed. 33,398 targets were identified from this initial screen. SAM was then applied with a false discovery rate (FDR) set to <5% (FDR 4.4%, delta value 1.17), equivalent to a p-value of <0.05. A full list of microarray data is accessible in GEO DataSets under accession no. GSE38010.

MS proteome. The protein expression datasets of MS and control samples are from a previously described study by Han et al. (2008). In brief, AP, CAP, and CP lesions were isolated by laser capture microdissection, and samples from the same lesion types were pooled and separated by SDS-PAGE analysis. Individual gel bands were digested with trypsin, and tryptic peptides were analyzed repeatedly by mass spectrometry (four to seven times) with a linear quadrupole (LTQ) ion-trap mass spectrometer. Data obtained from each gel band were originally searched against the nonredundant human protein database (Release 20041130 from Advanced Biomedical Computing Center) using the SEQUEST algorithm (Yates et al., 1995). Files from AP, CAP, and CP were then combined using INTERACT (Han et al., 2001) and filtered with XCorr scores of 1.9, 2.2, and 3.7 for 1+, 2+, and 3+ ions, Delta correlation >0.1 with false positive rate <1% excluding single peptide IDs. For the current study, these previously filtered peptides were researched against the human subset of the UniProt Knowledgebase Release 12.5 (13 November 2007) to update protein lists and corresponding spectral counts.

Comparative protein and RNA profiling. The semiquantitation of protein abundance was obtained by normalizing the mean spectral counts of each protein within a lesion type (control, AP, CAP, and CP) relative to the total mean spectral counts for the particular lesion type. Relative abundance of RNA expression was similarly obtained by normalizing mean fluorescent intensities relative to total mean intensities. Mean fluorescent intensity was calculated based on all probes mapping to a given target for duplicate microarray analyses, except in the case of the AP sample, where only one microarray analysis was performed. Logs (base 10) of relative abundance estimates were used to determine inliers (all lesion types showing less than one order of magnitude abundance differences), midliers (all lesion types showing at least one and less than two orders of magnitude abundance differences), and outliers (all remaining overlapping targets). Logs were normalized to a mean of zero within each lesion type for the creation of heat maps. The normalized logs were hierarchically clustered based on uncentered correlation with centroid linkage using Cluster 3.0 (Eisen et al., 1998) and visualized using Java TreeView (Saldanha, 2004).

EAE, treatment with mAb CD47, immune cell proliferation, and cytokine analysis. CD47$^{-/-}$ mice and WT C57BL/6 mice were housed in the Research Animal Facility at Stanford University. EAE was induced in 8–9-wk-old WT or CD47$^{-/-}$ mice (n = 9–10 per group) immunized with CFA and MOG$_{35–55}$ peptide and *Bordetella pertussis* toxin (400 ng per mouse i.p. injections; eBioscience) on days 0 and 2. For treatment with mAb against CD47 (mAb CD47), EAE was induced in C57BL/6 WT mice. Mice were treated with daily i.p. injections of 100 μg mAb CD47 or isotype control IgG at specified time points. Mice were followed clinically every day up to day 35. Mice were scored according to the following: 0, normal; 1, tail paralysis; 2, hindlimb weakness; 3, complete hindlimb paralysis; 4, hindlimb paralysis with forelimb weakness; and 5, moribund or death. Animal experiments were approved by and performed in compliance with the National Institutes of Health guidelines of the Institutional Animal Care and Use Committee at Stanford University.

Immune cell proliferation and cytokine analysis were performed as previously described (Ousman et al., 2007). In brief, splenocytes and lymph node cells from WT and CD47$^{-/-}$ mice were incubated in 96-well flat-bottom plates in stimulation media and activated with increasing concentrations of MOG$_{35–55}$ peptide. For proliferation assays, cells were pulsed with [^{3}H]thymidine at 48 h and harvested 16 h later on a filter using a cell harvester, and incorporated radioactivity was counted using a β scintillation counter. For cytokine analysis, immune cells were incubated for 24, 48, 72, 96, and 120 h, and cytokine levels were measured at different time points using anti–mouse ELISA kits (IL-2, IL-4, IL-6, IL-10, IL-12p40, IFN, and OptEIA [BD]; IL-17 and TNF [R&D Systems]).

Adoptive transfer. WT C57BL/6 or CD47$^{-/-}$ mice (female, 8–9 wk old) were immunized with CFA and MOG$_{35–55}$, and splenocytes and lymph node cells were harvested on day 9 after immunization and expanded in vitro with 10 μg/ml MOG and 20 ng/ml IL-12 (eBioscience) for 72 h. Cells were then harvested, washed once with prewarmed PBS, counted, and injected into either 5–6-wk-old RAG$^{-/-}$, WT, or CD47$^{-/-}$ recipient mice (50 × 10^6 cells per mouse) i.p. and followed clinically up to at least day 30. Pertussis toxin (400 ng/dose) was administered by i.p. injections on days 0 and 2.

Mixed lymphocyte assay. For lymphocyte mixing experiments, CD3$^+$ T lymphocytes from WT C57BL/6 or CD47$^{-/-}$ mice immunized with CFA and MOG$_{35–55}$ were harvested on day 9 after immunization after negative affinity selections by anti-CD3 affinity purification (BD). WT or CD47$^{-/-}$ CD3$^+$ cells were incubated in 96-well round-bottom plates (10^6 cells per well) with WT or CD47$^{-/-}$ irradiated splenocytes (3,000 RADS, 5 × 10^6 cells per well), pulsed with [^{3}H]thymidine at either 24, 48, or 72 h, and harvested 16 h later, and thymidine incorporation was counted using a β scintillation counter.

FACS analysis. For flow cytometry, splenocytes or lymph node cells from either naive or immunized WT and CD47$^{-/-}$ mice were labeled with mAbs against CD3, CD4, CD8, CD11b, CD11c, CD19, CD44, CD27, CD80,

and CD86 and analyzed by a two-color FACScan flow cytometer (BD). Data were analyzed using FlowJo software (Tree Star).

In vitro phagocytosis assay. Phagocytosis assays were performed as previously described (Jaiswal et al., 2009). Human myelin was isolated as described in Ishii et al. (2009). Female C57BL/6 mice were immunized subcutaneously with MOG$_{35-55}$/CFA. Mice were given an i.p. injection of Pertussis toxin at days 0 and 2. Splenocytes were harvested on day 9. CSFE-labeled myelin fraction (1 mg/ml) or EAE splenocytes were incubated with mouse macrophages in the presence of 10 µg/ml Ig2a isotype, anti–mouse CD47 (mIAP301), or anti–SIRP-α for 2 h. Cells were analyzed to determine the phagocytosis index (number of cells phagocytosed per 100 macrophages) by fluorescence microscopy. P < 0.05 was determined to be statistically significant by Student's *t* test.

Statistical analysis. Data represent means ± SEM. The Student's *t* test (*n* = 2 per groups) was used for parametric data. The Mann–Whitney *t* test was performed to detect between group differences. A p-value of <0.05 was rendered statistically significant.

Online supplemental material. Fig. S1 shows a flow chart of microarray and proteomic analysis of MS lesions. Fig. S2 shows the intersection of targets identified by microarray and proteomic analysis. Fig. S3 shows that CD47$^{-/-}$ T cells proliferate when activated with anti-CD3 or anti-CD28 in vitro. Fig. S4 shows that CD47$^{-/-}$ APCs express co-stimulatory molecules upon either LPS or CpG activation. Fig. S5 shows that mAb CD47 treatment lessens EAE severity. Fig. S6 shows a bone marrow chimera experiment. Table S1, included as an Excel file, shows the MS brain lesion transcriptome. Table S2, included as an Excel file, shows the MS brain lesion proteome. Table S3, included as an Excel file, compares the MS brain lesion transcriptome and proteome. Online supplemental material is available at http://www.jem.org/cgi/content/full/jem.20101974/DC1.

REFERENCES

Barres, B.A. 2008. The mystery and magic of glia: a perspective on their roles in health and disease. *Neuron.* 60:430–440. http://dx.doi.org/10.1016/j.neuron.2008.10.013

Bhat, R., R. Axtell, A. Mitra, M. Miranda, C. Lock, R.W. Tsien, and L. Steinman. 2010. Inhibitory role for GABA in autoimmune inflammation. *Proc. Natl. Acad. Sci. USA.* 107:2580–2585. http://dx.doi.org/10.1073/pnas.0915139107

Cahoy, J.D., B. Emery, A. Kaushal, L.C. Foo, J.L. Zamanian, K.S. Christopherson, Y. Xing, J.L. Lubischer, P.A. Krieg, S.A. Krupenko, et al. 2008. A transcriptome database for astrocytes, neurons, and oligodendrocytes: a new resource for understanding brain development and function. *J. Neurosci.* 28:264–278. http://dx.doi.org/10.1523/JNEUROSCI.4178-07.2008

Dutta, R., J. McDonough, X. Yin, J. Peterson, A. Chang, T. Torres, T. Gudz, W.B. Macklin, D.A. Lewis, R.J. Fox, et al. 2006. Mitochondrial dysfunction as a cause of axonal degeneration in multiple sclerosis patients. *Ann. Neurol.* 59:478–489. http://dx.doi.org/10.1002/ana.20736

Eisen, M.B., P.T. Spellman, P.O. Brown, and D. Botstein. 1998. Cluster analysis and display of genome-wide expression patterns. *Proc. Natl. Acad. Sci. USA.* 95:14863–14868. http://dx.doi.org/10.1073/pnas.95.25.14863

Frohman, E.M., M.K. Racke, and C.S. Raine. 2006. Multiple sclerosis—the plaque and its pathogenesis. *N. Engl. J. Med.* 354:942–955. http://dx.doi.org/10.1056/NEJMra052130

Griffiths, M.R., P. Gasque, and J.W. Neal. 2009. The multiple roles of the innate immune system in the regulation of apoptosis and inflammation in the brain. *J. Neuropathol. Exp. Neurol.* 68:217–226. http://dx.doi.org/10.1097/NEN.0b013e3181996688

Gygi, S.P., B. Rist, and R. Aebersold. 2000. Measuring gene expression by quantitative proteome analysis. *Curr. Opin. Biotechnol.* 11:396–401. http://dx.doi.org/10.1016/S0958-1669(00)00116-6

Han, D.K., J. Eng, H. Zhou, and R. Aebersold. 2001. Quantitative profiling of differentiation-induced microsomal proteins using isotope-coded affinity tags and mass spectrometry. *Nat. Biotechnol.* 19:946–951. http://dx.doi.org/10.1038/nbt1001-946

Han, M.H., S.I. Hwang, D.B. Roy, D.H. Lundgren, J.V. Price, S.S. Ousman, G.H. Fernald, B. Gerlitz, W.H. Robinson, S.E. Baranzini, et al. 2008. Proteomic analysis of active multiple sclerosis lesions reveals therapeutic targets. *Nature.* 451:1076–1081. http://dx.doi.org/10.1038/nature06559

Ishii, A., R. Dutta, G.M. Wark, S.I. Hwang, D.K. Han, B.D. Trapp, S.E. Pfeiffer, and R. Bansal. 2009. Human myelin proteome and comparative analysis with mouse myelin. *Proc. Natl. Acad. Sci. USA.* 106:14605–14610. http://dx.doi.org/10.1073/pnas.0905936106

Jaiswal, S., C.H. Jamieson, W.W. Pang, C.Y. Park, M.P. Chao, R. Majeti, D. Traver, N. van Rooijen, and I.L. Weissman. 2009. CD47 is upregulated on circulating hematopoietic stem cells and leukemia cells to avoid phagocytosis. *Cell.* 138:271–285. http://dx.doi.org/10.1016/j.cell.2009.05.046

Junker, A., M. Krumbholz, S. Eisele, H. Mohan, F. Augstein, R. Bittner, H. Lassmann, H. Wekerle, R. Hohlfeld, and E. Meinl. 2009. MicroRNA profiling of multiple sclerosis lesions identifies modulators of the regulatory protein CD47. *Brain.* 132:3342–3352. http://dx.doi.org/10.1093/brain/awp300

Kanter, J.L., S. Narayana, P.P. Ho, I. Catz, K.G. Warren, R.A. Sobel, L. Steinman, and W.H. Robinson. 2006. Lipid microarrays identify key mediators of autoimmune brain inflammation. *Nat. Med.* 12:138–143. http://dx.doi.org/10.1038/nm1344

Kislinger, T., B. Cox, A. Kannan, C. Chung, P. Hu, A. Ignatchenko, M.S. Scott, A.O. Gramolini, Q. Morris, M.T. Hallett, et al. 2006. Global survey of organ and organelle protein expression in mouse: combined proteomic and transcriptomic profiling. *Cell.* 125:173–186. http://dx.doi.org/10.1016/j.cell.2006.01.044

Koning, N., L. Bö, R.M. Hoek, and I. Huitinga. 2007. Downregulation of macrophage inhibitory molecules in multiple sclerosis lesions. *Ann. Neurol.* 62:504–514. http://dx.doi.org/10.1002/ana.21220

Lamy, L., A. Foussat, E.J. Brown, P. Bornstein, M. Ticchioni, and A. Bernard. 2007. Interactions between CD47 and thrombospondin reduce inflammation. *J. Immunol.* 178:5930–5939.

Lassmann, H., W. Brück, and C. Lucchinetti. 2001. Heterogeneity of multiple sclerosis pathogenesis: implications for diagnosis and therapy. *Trends Mol. Med.* 7:115–121. http://dx.doi.org/10.1016/S1471-4914(00)01909-2

Lock, C., G. Hermans, R. Pedotti, A. Brendolan, E. Schadt, H. Garren, A. Langer-Gould, S. Strober, B. Cannella, J. Allard, et al. 2002. Gene-microarray analysis of multiple sclerosis lesions yields new targets validated in autoimmune encephalomyelitis. *Nat. Med.* 8:500–508. http://dx.doi.org/10.1038/nm0502-500

Lu, P., C. Vogel, R. Wang, X. Yao, and E.M. Marcotte. 2007. Absolute protein expression profiling estimates the relative contributions of transcriptional and translational regulation. *Nat. Biotechnol.* 25:117–124. http://dx.doi.org/10.1038/nbt1270

Majeti, R., M.P. Chao, A.A. Alizadeh, W.W. Pang, S. Jaiswal, K.D. Gibbs Jr., N. van Rooijen, and I.L. Weissman. 2009. CD47 is an adverse prognostic factor and therapeutic antibody target on human acute myeloid leukemia stem cells. *Cell.* 138:286–299. http://dx.doi.org/10.1016/j.cell.2009.05.045

Menon, K., M.N. Rasband, C.M. Taylor, P. Brophy, R. Bansal, and S.E. Pfeiffer. 2003. The myelin-axolemmal complex: biochemical dissection and the role of galactosphingolipids. *J. Neurochem.* 87:995–1009. http://dx.doi.org/10.1046/j.1471-4159.2003.02075.x

Ousman, S.S., B.H. Tomooka, J.M. van Noort, E.F. Wawrousek, K.C. O'Connor, D.A. Hafler, R.A. Sobel, W.H. Robinson, and L. Steinman. 2007. Protective and therapeutic role for alphaB-crystallin

in autoimmune demyelination. *Nature*. 448:474–479. http://dx.doi.org/10.1038/nature05935

Robinson, W.H., C. DiGennaro, W. Hueber, B.B. Haab, M. Kamachi, E.J. Dean, S. Fournel, D. Fong, M.C. Genovese, H.E. de Vegvar, et al. 2002. Autoantigen microarrays for multiplex characterization of autoantibody responses. *Nat. Med*. 8:295–301. http://dx.doi.org/10.1038/nm0302-295

Saldanha, A.J. 2004. Java Treeview—extensible visualization of microarray data. *Bioinformatics*. 20:3246–3248. http://dx.doi.org/10.1093/bioinformatics/bth349

Shatz, C.J. 2009. MHC class I: an unexpected role in neuronal plasticity. *Neuron*. 64:40–45. http://dx.doi.org/10.1016/j.neuron.2009.09.044

Steinman, L. 2004. Elaborate interactions between the immune and nervous systems. *Nat. Immunol*. 5:575–581. http://dx.doi.org/10.1038/ni1078

Stevens, B., N.J. Allen, L.E. Vazquez, G.R. Howell, K.S. Christopherson, N. Nouri, K.D. Micheva, A.K. Mehalow, A.D. Huberman, B. Stafford, et al. 2007. The classical complement cascade mediates CNS synapse elimination. *Cell*. 131:1164–1178. http://dx.doi.org/10.1016/j.cell.2007.10.036

Tusher, V.G., R. Tibshirani, and G. Chu. 2001. Significance analysis of microarrays applied to the ionizing radiation response. *Proc. Natl. Acad. Sci. USA*. 98:5116–5121. http://dx.doi.org/10.1073/pnas.091062498

Wu, L., S.I. Hwang, K. Rezaul, L.J. Lu, V. Mayya, M. Gerstein, J.K. Eng, D.H. Lundgren, and D.K. Han. 2007. Global survey of human T leukemic cells by integrating proteomics and transcriptomics profiling. *Mol. Cell. Proteomics*. 6:1343–1353. http://dx.doi.org/10.1074/mcp.M700017-MCP200

Yates, J.R. III, J.K. Eng, and A.L. McCormack. 1995. Mining genomes: correlating tandem mass spectra of modified and unmodified peptides to sequences in nucleotide databases. *Anal. Chem*. 67:3202–3210. http://dx.doi.org/10.1021/ac00114a016